Available online at www.sciencedirect.com
SCIENCE DIRECT®
Journal of Nuclear Materials 322 (2003) 165–179
journal of nuclear materials
www.elsevier.com/locate/jnucmat

Crystal structures of curium compounds: an ab initio study

V. Milman [a,*], B. Winkler [b], C.J. Pickard [c]

[a] *Accelrys Inc., 334 Science Park, Cambridge CB4 0WN, UK*
[b] *Institut für Mineralogie Abt. Kristallographie, Johann Wolfgang Goethe-Universität, Senckenberganlage 30, D 60054 Frankfurt a. M., Germany*
[c] *Theory of Condensed Matter, Cavendish Laboratory, Madingley Road, Cambridge CB3 0HE, UK*

Received 16 January 2003; accepted 26 June 2003

Abstract

The crystal structure and electronic properties of curium and its compounds are investigated using the density functional theory approach. The accuracy of the method is shown to be sufficient to describe structures with various types of chemical bonding: halides, pnictides, oxides, hydrides and intermetallic compounds. Selected examples are given of the studies of properties and phase stability of curium compounds under hydrostatic compression. Further applications of the theoretical approach to crystallography and solid state chemistry of actinides are suggested.

1. Introduction

Since their discovery, there has been a continuing interest in the crystal chemistry of the actinide elements and their compounds. This interest has had both fundamental and applied aspects. In the case of curium, which is the subject of the present investigation, there are numerous open questions ranging from the accurate determination of crystal structures and magnetic properties of curium compounds to the investigation of the nature of curium ions in various oxidation states [1,2].

Curium is the heaviest actinide element for which multigram quantities are available for chemical and crystallographic studies. The most stable curium isotope, ^{248}Cm, is only available in milligram samples, however, which makes accurate structural investigations extremely challenging. A large number of structural data for curium compounds has been obtained using a more abundant isotope ^{244}Cm. Unfortunately, in this case self-irradiation has a detrimental effect on the structure of ^{244}Cm compounds. It has been shown, for example, that the lattice parameter of $^{244}CmO_2$ increases by about 0.2% in one day [3], and radiation-induced phase transitions have been reported as well [1,4]. Experimental studies face additional difficulties related to the presence of the traces of other actinides such as americium in curium samples, to the high defect concentration, and to deviations from stoichiometry caused by radiation damage.

These factors combined make a compelling case for theoretical studies of curium compounds as an additional source of structural and chemical information. Historically this approach has had its successes and its difficulties when applied to *f*-elements. First of all, only first principles studies can be sufficiently accurate for this purpose. The most popular scheme for ab initio studies of complex structures is based on the density functional theory (DFT) [5] and on the plane wave pseudopotential approach [6,7]. The two questions are usually raised by this combination, namely (i) how accurate is the DFT description of *f*-electron systems, and (ii) whether the pseudopotential approach is sufficiently robust for such systems.

Recently Söderlind et al. showed that gradient corrected density functionals work well for a series of *f*-electron metals [8,9]. Pickard et al. [10] subsequently demonstrated that the ultrasoft Vanderbilt

* Corresponding author. Tel.: +44-1223 228500/228619; fax: +44-1223 228501.
E-mail address: vmilman@accelrys.com (V. Milman).

0022-3115/$ - see front matter © 2003 Elsevier B.V. All rights reserved.
doi:10.1016/S0022-3115(03)00321-0

pseudopotentials [11] can be used to calculate structural parameters and elastic constants of compounds containing 4*f* and 5*f* electrons reliably.

In this paper we present the results of an ab initio study of a number of curium compounds, aiming to build further confidence in this approach and to provide important crystal chemical information for a wide variety of curium-containing crystals. Theoretical data in this area can usefully supplement experiment in various cases where single-crystal X-ray diffraction determination of the atomic coordinates is not possible; in some cases even the space group of a compound cannot be determined unambiguously. An additional motivation is that the latest comprehensive review of crystal structure and solid-state chemistry of curium compounds [1] is getting out of date, especially in the area of intermetallic compounds of curium. We provide a critical review of the latest relevant experimental work highlighting existing controversial issues.

2. Computational details

The quantum-mechanical calculations performed here are based on DFT [5]. While DFT itself is exact, practical calculations require an approximation for the treatment of the exchange and correlation energies. Here we use the generalised gradient approximation, GGA [12], as implemented in Ref. [13]. We used the spin-polarized version of the PBE form of the GGA [14], which was designed to be more robust and accurate than the original GGA formulation.

The computational scheme that we use here is based on an expansion of the charge density and electronic wavefunctions in a basis set of plane waves. However, as it is impractical to consider tightly bound core electrons explicitly when using a plane-wave basis set, pseudopotentials have to be used to mimic the screening of the Coulomb potential of the nucleus by the core electrons.

A number of approaches for the construction of pseudopotentials have been presented in the literature [6,7]. The state-of-the-art are the efficient 'ultrasoft' pseudopotentials, leading to calculations that require a comparatively small number of plane waves [11]. Such ultrasoft pseudopotentials were used here, with a maximum cutoff energy of the plane waves of 400 eV. The potentials were extended so that non-local projectors were available up to $l = 3$ allowing *f*-electrons to be accurately described [10]. To obtain transferable pseudopotentials, the so-called 'shallow-core' electrons are treated as valence electrons (for example, the 6*s* and 6*p* electrons for curium). In order to optimize the structures it is essential to calculate the first derivatives of the total energy – the forces and stresses. The expressions required for the case of ultrasoft pseudopotentials have been summarized by Focher and Chiarotti [15].

In addition to the cutoff energy, only one further parameter determines the quality of the calculations, namely the density of points with which the Brillouin zone is sampled. Here we use a sampling of reciprocal space such that distances between grid points are less than 0.4 nm^{-1}. The cell parameters are converged to approximately 0.0001 nm with the described settings.

The particular implementation of the plane-wave pseudopotential code used in this work is CASTEP [7,16]. The majority of the calculations were carried out using CASTEP 2.1, while a few intermetallic compounds were studied using the later version CASTEP 2.2 [17]. The pseudopotentials were taken from the standard database distributed with this package. All the results presented below were obtained using the pseudopotentials generated using the local density approximation for exchange-correlation functional. The results obtained with the PBE-generated potentials are qualitatively similar, but the interatomic distances tend to be 0.5–1% longer.

No attempt is made here to model the spin–orbit terms that might be large in these systems. This explains the discrepancies between calculated and measured effective magnetic moments. There is also a possibility that the spin–orbit interactions are so strong as to affect the crystal structure of the ground state. The results given in the following sections suggest that this is not the case; the errors we observe are typical for the DFT description of non-magnetic substances [7].

The present calculations are restricted to the athermal limit, in which temperature effects and zero-point atomic motion are neglected. We always attempt to compare our results to low-temperature experimental data. The estimated errors in structural parameters due to the neglect of the thermal expansion are less than 0.1% when we compare theoretical values at 0 K to experimental room temperature results. This effect is negligible in the context of the present study and will be always masked by either the DFT error (of the order of 1%) or the radiation damage effects.

The neglect of the finite temperature effects is more important for the evaluation of the phase stability of curium compounds. The enthalpy differences quoted below give only the rough guide to the free energy differences, assuming that the vibrational properties of the phases involved and thus the entropic contributions to the free energy are generally similar.

3. Results and discussion

3.1. Metallic curium

Curium metal exists in two modifications, a double hexagonal close-packed (dhcp) structure of the α-La type ($P6_3/mmc$, SG 194), and a high-temperature fcc

structure ($Fm\bar{3}m$, SG 225) [1]. The temperature of the dhcp-to-fcc transition is not known; it is believed to be about 50 K below the melting point, $T_m = 1620$ K [18]. The lattice parameters of the dhcp polymorph of ^{244}Cm are reported as $a = 0.3496(3)$ and $c = 1.1331(5)$ nm [1], or 0.3494 and 1.1334 nm [19]. More recent measurement gives the values of 0.35015 and 1.13804 nm for ^{248}Cm samples [20]. Our result is $a = 0.3647$ and $c = 1.1820$ nm, overestimating both lattice parameters by about 4% (the c/a ratio is reproduced to better than 0.2%).

High-temperature fcc polymorph of curium has been reported to have the lattice parameter at room temperature between 0.5039(2), 0.5065 [1], and 0.51429 nm [20]. CASTEP result of $a = 0.5045$ nm is in good agreement with these findings. The calculations suggest that the two structures nearly degenerate energetically. The dhcp Cm modification is found to be more stable by only 0.2 kJ/mol, which implies that entropic effects are important for the accurate description of this transition. The degeneracy explains the high stability of the fcc phase at room temperature: Damien et al. [21] reported that it was impossible to remove traces of the fcc Cm from their dhcp samples and vice versa.

It is likely that the discrepancy between the calculated and measured lattice parameters of the dhcp polymorph is related to the difficulty of describing the antiferromagnetic ground state of this structure. CASTEP finds a ferromagnetic ground state for both fcc and dhcp structures, in both cases with a magnetic moment of about 7.7 μ_B/atom. This value agrees with the prediction of 7.94 μ_B/atom for the f^7 configuration of curium atom based on the L–S coupling and Hund's rule [20], and with the experimentally measured values from 7.85 to 8.10 μ_B/atom [19]. In reality the dhcp phase is antiferromagnetic with a Néel temperature of 65 K, and it has a second magnetic transition at about 200 K. The fcc modification has a ferrimagnetic transition at about 200 K [20]. It follows that CASTEP predicts correct magnetic moments on atoms, but fails to reproduce their ordering. In view of the large magnitude of magnetic moments, it is possible that this failure is responsible for the discrepancy in lattice parameters.

3.2. Curium halides and related compounds

Halides of trivalent and tetravalent curium represent the most extensively studied and most accurately characterized class of curium compounds [1]. The results of structural investigations of these compounds are presented below.

3.2.1. Curium trichloride

Curium trichloride has the hexagonal UCl_3-type structure, space group $P6_3/m$ (SG 176, $Z = 2$). The reported experimental structure for $^{248}CmCl_3$ is compared to the present theoretical results in Table 1. CASTEP results deviate from the measured data by less than 3%, which is similar to the accuracy reported in the theoretical study of various compounds of *f*-elements [10].

Each Cm atom has nine Cl neighbors in this structure. Cl atoms are in the corners of a trigonal prism, Cl(1), with three equatorial atoms centered over the three faces of the prism, Cl(2). The Cm–Cl(1) distances are slightly shorter than the equatorial distances, see Table 1. The main discrepancy between the calculated and experimental structure is in the value of the *a* cell parameter and correspondingly in the Cm–Cl(2) distance. It is likely that, similar to the case of metallic curium, the wrong description of these distances is related to the overestimation of the magnetic interaction in the predicted ferromagnetic ground state.

Curium trichloride has been recently shown to transform to an orthorhombic $PuBr_3$-type structure under pressure of about 6 GPa, and possibly to a new unidentified phase at about 11 GPa [24]. We found that the hexagonal modification is more stable than the orthorhombic one by $\Delta H = 23.7$ kJ/mol at ambient pressure. We suggest that ab initio modeling offers a reliable tool to study this sequence of transitions (see also Section 3.5.1, CmBi).

3.2.2. Curium tribromide

Curium tribromide crystallizes in the orthorhombic $PuBr_3$-type structure, space group C*mcm* (SG 63, $Z = 4$). Experimental and calculated structural parameters are

Table 1
Theoretical and experimental structure of $CmCl_3$

	Experimental [22]	Experimental [23]	Theory
a, nm	0.73743(11)	0.7368(6)	0.7263 (−1.5%)
c, nm	0.41850(7)	0.4228(4)	0.4141 (−1.1%)
V, nm^3	0.1971	0.1988	0.1891
Cl_x	0.3882(2)	–	0.3825
Cl_y	0.3018(2)	–	0.2974
Cm–Cl(1)×6, nm	0.28589(9)	–	0.2842 (−0.6%)
Cm–Cl(2)×3, nm	0.29138(13)	–	0.2877 (−1.3%)

The curium atom is on the Wyckoff 2*c* position with coordinates (1/3, 2/3, 1/4), chlorine is on the 6*h* position with coordinates (Cl_x, Cl_y, 1/4).

Table 2
Theoretical and experimental structure of $CmBr_3$

	Experimental [2]	Experimental [23]	Theory (0 GPa)	Theory (0.5 GPa)
a, nm	0.4041(2)	0.4048(2)	0.4048 (+0.2%)	0.4021 (−0.5%)
b, nm	1.270(2)	1.266(1)	1.3353 (+5.1%)	1.2615 (−0.6%)
c, nm	0.9135(3)	0.9124(7)	0.9147 (+0.1%)	0.9042 (−1.0%)
V, nm^3	0.4688	0.4676	0.4944	0.4587
Cm_y	0.2431(2)	–	0.2408	0.2402
$Br1_y$	0.5831(6)	–	0.5876	0.5781
$Br2_y$	0.1461(4)	–	0.1506	0.1450
$Br2_z$	0.5658(4)	–	0.5668	0.5655
Cm–Br(1)×2, nm	0.2865(6)	–	0.2877 (+0.4%)	0.2864 (0.0%)
Cm–Br(2)×4, nm	0.2983(4)	–	0.3002 (+0.6%)	0.2987 (+0.1%)
Cm–Br(2)×2, nm	0.3137(4)	–	0.3138 (0.0%)	0.3096 (−1.3%)

The curium atom is on the Wyckoff 4c position with coordinates (0, Cm_y, 1/4), the bromine atoms are on the positions 4c with coordinates (0, $Br1_y$, 1/4) and 8f with coordinates (0, $Br2_y$, $Br2_z$). CASTEP results are shown at zero and 0.5 GPa external pressure.

given in Table 2. $CmBr_3$ has a layered structure with weak interactions between the layers. It is well known that the DFT description of dispersion forces, which are responsible for interlayer interactions, is not sufficiently accurate. This is illustrated by the data in Table 2 where we compare the results of the structure optimization carried out at ambient conditions and under small external pressure. The fact that the application of just 0.5 GPa external pressure changes the c parameter by about 5% confirms that the energy dependence on the interlayer separation is weak and the minimum that corresponds to the ground state is very shallow.

The structure of the CmBr layers is reproduced accurately in the calculations, both at 0 GPa and under small compression (Table 2). Each Cm ion is surrounded by eight Br ions. The decrease in coordination number when compared to $CmCl_3$ is related to the larger ionic radius of the Br ions.

3.2.3. Curium triiodide

Curium triiodide has a trigonal BiI_3-type structure, space group $R\bar{3}$ (SG 148, $Z = 6$). This is a layered structure composed of the layers of edge-sharing octahedra. The trend towards decreasing coordination number of Cm as the size of the anion increases is clearly revealed here, as Cm in CmI_3 is only sixfold coordinated, compared to the coordination numbers of eight and nine for tribromide and trichloride, respectively. The octahedra within the layers are slightly distorted as can be seen from the small differences between the two sets of Cm–I bond lengths (Table 3). The iodide compounds of actinides are less stable than other halides [23], which explains the lack of high quality experimental data for this compound.

3.2.4. Curium trifluoride

The crystal structure of curium trifluoride is still being discussed with a certain amount of controversy. The structure was reported by Aprey et al. [23] as hexagonal of the LaF_3-type, space group $P6_3/mmc$ (SG 194, $Z = 2$). In fact, LaF_3 or tysonite structure is trigonal with the space group of $P\bar{3}c1$ (SG 165, $Z = 6$) [25,26]. The trigonal description of CmF_3 was later used by other authors [1,2]. The a_t cell parameter for the trigonal structure quoted by Brown [2] is based directly on the earlier data of Aprey et al. [23]. Its value is obtained from the a_h cell parameter in the hexagonal setting as $a_t = a_h\sqrt{3}$. The trigonal description can be actually seen as a more complex (defect) structure of LaF_3. We carried out the calculations in both of these space groups and found that the trigonal cell is more stable than the hexagonal one by $\Delta H = 9.1$ kJ/mol. The structure of CmF_3 as obtained using both hexagonal and trigonal descriptions is given in Tables 4 and 5.

Table 3
Theoretical and experimental structure of CmI_3 (hexagonal setting)

	Experimental [23]	Theory
a, nm	0.744(9)	0.7740 (+4.0%)
c, nm	2.04(1)	2.0684 (+1.4%)
V, nm^3	0.978	1.0731
I_x	–	0.3394
I_y	–	0.3298
I_z	–	0.0817
Cm–I(1)×3, nm	–	0.3095
Cm–I(2)×3, nm	–	0.3109

The curium atom is on the Wyckoff 6c position with coordinates (0, 0, 1/6), iodine is on the 18f position with coordinates (I_x, I_y, I_z). No experimental single-crystal data exists for CmI_3.

The Cm atom in the hexagonal cell has three short bonds to F2 atoms in the (0 0 1) plane, two slightly longer bonds along the (0 0 1) direction to F1 atoms, and further six longer bonds to F1 atoms. This spatial arrangement results in a very high coordination number,

Table 4
Theoretical and experimental structure of CmF_3 in the hexagonal cell (SG 194)

	Experimental [23]	Theory
a, nm	0.4041(1)	0.4100 (+1.5%)
c, nm	0.7179(2)	0.7289 (+1.5%)
V, nm^3	0.1015	0.1061
$F1_z$	–	0.0786
Cm–F(2)×3, nm	–	0.2367
Cm–F(1)×2, nm	–	0.2395
Cm–F(1)×6, nm	–	0.2676

The unit cell contains Cm on 2*c* (2/3, 1/3, 1/4), F1 on 4*f* (1/3, 2/3, $F1_z$), and F2 on 2*a* (0, 0, 1/4).

$C_N = 11$, and in a large number of relatively weak long bonds. The curium coordination in the trigonal cell is more compact than in the hexagonal cell with the same coordination number, nine, as in the $CmCl_3$ cell. The comparison of bond lengths in Tables 4 and 5 shows that the six long bonds found in the hexagonal structure disappear in the trigonal cell. This change in Cm coordination provides a plausible explanation for the energy stabilization of the trigonal cell.

3.2.5. Curium oxychloride

CmOCl crystallizes in the tetragonal PbClF-type structure, space group P4/*nmm* (SG 129) [27] (Table 6). The structure consists of layers of coplanar oxygen atoms and coplanar chlorine atoms arranged in repeating units of O–Cl–Cl. The metal atoms are found in the interstices between the oxygen and chlorine layers. Each Cm atom is ninefold coordinated, as in curium trichloride. Curium forms four bonds to the oxygen layer, four bonds to the adjacent chlorine layer, and one bond to the second chlorine layer. Cm–Cl bonds in oxychloride are longer than in chloride, indicating that the Cm–O interaction is stronger than the Cm–Cl one.

3.2.6. Curium tetrafluoride

CmF_4 is the only simple halide compound of tetravalent curium [1,2]. The structure has been described as a monoclinic ZrF_4-type, space group C2/*c* (SG 15). This compound is isostructural with a number of other actinide tetrafluorides [29]. Each Cm atom in the structure is eightfold coordinated in a distorted antiprism configuration. The details of the structure are given in Table 7 where atomic coordinates of CmF_4 are compared to those determined for the isostructural compound UF_4 [29]. Analysis of the table confirms close similarity between CmF_4 and UF_4 structures; the fractional coordinates are essentially the same for all the atoms. The overall agreement between calculated and experimental data is very good for this structure, perhaps the most crystallographically complex one in the present study. The remaining discrepancies are consistent with the overall accuracy of the DFT modeling, especially since synthesized CmF_4 is likely to have a non-stoichiometric defect structure [1].

3.3. Curium hydrides

Curium dihydride has been prepared and characterized by Bansal and Damien [30], and later by Gibson and Haire [31]. Material prepared in the early work has been tentatively classified as CmH_{2+x}, $0 \leqslant x \leqslant 0.7$, in analogy with Np, Pu and Am hydrides [30]. The structure was described as having a fluorite-type lattice with $a = 0.5344(5)$ nm. The present calculation gives 0.5382 nm, which is only 0.7% higher than the reported value. A more recent study reports the same compound to have

Table 5
Theoretical and experimental structure of CmF_3 in the trigonal cell (SG 165)

	Experimental [2]	Experimental ^{244}Cm [1]	Experimental ^{248}Cm [1]	Theory
a, nm	0.6999	0.7019(2)	0.7014(2)	0.7084 (+1.0%)
c, nm	0.7179	0.7198(2)	07194(2)	0.7259 (+0.9%)
V, nm^3	0.3046	0.3071	0.3065	0.3155
$F1_x$	–	–	–	0.3720
$F1_y$	–	–	–	0.0635
$F1_z$	–	–	–	0.0796
$F1_z$	–	–	–	0.1846
Cm_x	–	–	–	0.6569
Cm–F(2)×2, nm	–	–	–	0.2376
Cm–F(1)×2, nm	–	–	–	0.2424
Cm–F(1)×2, nm	–	–	–	0.2429
Cm–F(3)×1, nm	–	–	–	0.2431
Cm–F(1)×2, nm	–	–	–	0.2591

The curium atom is on the Wyckoff 6*f* position with coordinates (Cm_x, 0, 1/4), fluorine atoms are: F1 on the 12*g* position with coordinates ($F1_x$, $F1_y$, $F1_z$), F2 on 4*d* position with coordinates (1/3, 2/3, $F2_z$), and F3 on 2*a* position with coordinates (0, 0, 1/4). The errors in calculated cell parameters are relative to the ^{248}Cm experimental data.

Table 6
Theoretical and experimental structure of CmOCl

	Experimental [29]	Theory
a, nm	0.3985(3)	0.4015 (+0.8%)
c, nm	0.6752(8)	0.6760 (+0.1%)
V, nm^3	0.1072	0.1090
Cm_z	0.18[a]	0.1800
Cl_z	0.635[a]	0.6255
Cm–O×4, nm	0.233	0.2347
Cm–Cl×4, nm	0.308	0.3129
Cm–Cl×1, nm	0.307	0.3011

The unit cell contains Cm on 2c (0, 1/2, Cm_z), Cl on 2c (0, 1/2, Cl_z), and O on 2a (0, 0, 0). Bond lengths given by Peterson [27] are estimated based on the atomic coordinates of isostructural compounds AmOCl and CeOCl [28].

[a] Fractional coordinates are for CeOCl [28].

a lattice constant of 0.5322 nm, again in the fcc fluorite structure [31].

The distances between Cm atoms in curium dihydride are only slightly longer than in dhcp Cm, 0.381 nm compared to 0.363 nm. Thus magnetic and electronic properties of CmH_2 are reminiscent of pure Cm. Both materials are metallic with high density of states on the Fermi level. The magnetic moment of Cm atoms in CmH_2 is 7.5 μ_B/atom, higher than in halides and close to the results obtained for pure curium.

Gibson and Haire [32] used Knudsen effusion mass spectrometry to measure the dissociation enthalpy of curium dihydride. The reported value is 187(14) kJ/mol at 770 K. In order to compare this value to the theoretically calculated one, the dissociation enthalpy has to be extrapolated to zero temperature. By applying an empirical correction of the form $3/2RT$ we get the experimental value of $\Delta H(T=0) = 177(14)$ kJ/mol. Theoretical estimate of this quantity is obtained as

$$\Delta H = E(CmH_2) - E(Cm) - E(H_2), \quad (1)$$

where $E(CmH_2) = -2656.72$ eV and $E(Cm) = -2623.40$ eV from CASTEP calculations. The energy of the hydrogen molecule, $E(H_2)$, is evaluated using a supercell geometry as −31.70 eV. Substituting the theoretical values in Eq. (1) we obtain $\Delta H = 156$ kJ/mol in quantitative agreement with the experiment.

There are controversial reports regarding the stability of trivalent curium hydride, CmH_3. Bansal and Damien [30] have seen no sign of this allegedly hexagonal com-

Table 7
Theoretical and experimental structure of CmF_4

	Experiment [1,29]	Theory
a, nm	1.2500(9)	1.2612 (+0.9%)
b, nm	1.488(10)	1.0662 (+1.6%)
c, nm	0.8183(6)	0.8284 (+1.2%)
β, deg	126.10(5)	126.30 (+0.2%)
V, nm^3	0.8668	0.8977
Cm1 (4e)	0, 0.2131, 0.25	0, 0.2117, 0.25
Cm2 (8f)	0.2044, 0.4277, 0.8307	0.2051, 0.4273, 0.8315
F1 (4c)	0.25, 0.25, 0	0.25, 0.25, 0
F2 (4e)	0, 0.6041, 0.25	0, 0.6042, 0.25
F3 (8f)	0.8935, 0.2937, 0.9315	0.8934, 0.2936, 0.9312
F4 (8f)	0.8800, 0.0543, 0.0432	0.8800, 0.0540, 0.0431
F5 (8f)	0.7887, 0.5303, 0.8952	0.7886, 0.5306, 0.8951
F6 (8f)	0.6182, 0.1211, 0.7813	0.6185, 0.1211, 0.7814
F7 (8f)	0.6252, 0.3472, 0.6526	0.6248, 0.3471, 0.6520
Cm2–F5×1, nm	0.2184	0.2215 (+1.4%)
Cm2–F1×1, nm	0.2188	0.2218 (+1.4%)
Cm2–F6×1, nm	0.2219	0.2237 (+0.8%)
Cm2–F7×1, nm	0.2219	0.2258 (+1.8%)
Cm2–F3×1, nm	0.2232	0.2261 (+1.3%)
Cm2–F5×1, nm	0.2237	0.2263 (+1.2%)
Cm2–F2×1, nm	0.2255	0.2277 (+1.0%)
Cm2–F4×1, nm	0.2260	0.2278 (+0.8%)
Cm1–F6×2, nm	0.2197	0.2232 (+1.6%)
Cm1–F4×2, nm	0.2213	0.2240 (+1.2%)
Cm1–F7×2, nm	0.2226	0.2246 (+0.9%)
Cm1–F3×2, nm	0.2278	0.2311 (+1.4%)

The fractional coordinates reported in the experimental study [29] are for the UF_4 compound.

pound, while Gibson and Haire [31,32] reported observing hexagonal CmH_3 with $a = 0.3769(8)$, $c = 0.6732(12)$ nm in their experiments. They were unable to solve the structure in view of the experimental difficulties of detecting hydrogen atoms in compounds with heavy atoms while using the X-ray diffraction technique. CmH_3 was described as isostructural with Np, Pu and Am trihydrides [31], which implies the LaF_3-type lattice. This lattice type description creates the same problem as discussed above for CmF_3, namely, whether to use the hexagonal [31] or trigonal [1] version of the LaF_3 lattice when describing curium trihydride. We found that the two structures were nearly degenerate in enthalpy: the trigonal cell is only $\Delta H = 0.9$ kJ/mol more stable. The cell parameters in either representation are significantly lower than the experimental values. We obtained for the hexagonal cell $a = 0.3684$, $c = 0.6505$ nm, and the trigonal cell has very similar parameters: $a/\sqrt{3} = 0.3664$, $c = 0.6506$ nm. The only experimental report available gives the hexagonal cell of CmH_3 as $a = 0.3769(8)$, $c = 0.6732(12)$ nm [31]. The theoretical structure thus shows a nearly uniform compression by about 3% when compared to the experimental one.

We carried out analysis of the thermodynamical stability of CmH_3 along the same lines as described above for CmH_2, see Eq. (1). It appears that CmH_3 is unstable with respect to metallic curium and gas-phase hydrogen; the positive formation enthalpy is in this case $\Delta H = 45$ kJ/mol. This conclusion is consistent with the earlier experimental result where attempts to synthesize CmH_3 were unsuccessful [30]. There are thus compelling arguments for revisiting the structure of CmH_3: large discrepancy between the calculated and measured cell parameters, unfavourable energetics, and failure to produce this compound in other experiments. Further theoretical and experimental studies are required to shed light on the nature and thermodynamic stability of CmH_3.

3.4. Curium chalcogenides

This chapter presents the results for curium compounds with sulfur, selenium and tellurium. There is a rich variety of intermediate and possibly metastable phases in these systems, that might become a subject of a theoretical study in the future.

3.4.1. Cm–S compounds

Curium monosulfide has a cubic NaCl-type structure ($Fm\bar{3}m$, SG 225). Experimentally reported lattice parameter is 0.55754(6) nm [21]. The calculated value, 0.5648 nm, agrees well with this result (deviation of 1.3%). The Cm–S bond length is thus 0.2824 nm compared to the measured value of 0.2788 nm. CmS is found to be weakly metallic.

Curium disulfide crystallizes in the tetragonal lattice of anti-Fe_2 As type, space group P4/*nmm* (SG 129) [33]. The calculated structure is compared to the experimental results in Table 8. CmS_2 is also metallic, with a slightly higher density of electronic states at the Fermi level than CmS. The magnetic moment on Cm atom is slightly lower than in curium monosulfide.

Curium sesquisulfide, Cm_2S_3, has been characterized as a defect body-centered cubic phase of the anti-Th_3P_4 type with $a = 0.8452(5)$ nm [33]. No theoretical study of this compound has been undertaken here since the structure is too complex and most likely disordered. The stoichiometry of this phase could be anything between Cm_2S_3 and Cm_3S_4 [21], thus modeling of this system is practically impossible.

3.4.2. Cm–Se compounds

Curium selenides are in many respects similar to curium sulfides, except that the cell parameters and bond lengths are larger to reflect a bigger atomic radius of selenium. CmSe has a cubic NaCl-type structure with the lattice parameter of 0.5798(1) nm ($Fm\bar{3}m$, SG 225)

Table 8
Theoretical and experimental structure of curium dichalcogenides, CmM_2 (M = S, Se, Te)

	CmS_2		$CmSe_2$		$CmTe_2$	
	Experimental [33]	Theory	Experimental [33]	Theory	Experimental [34]	Theory
a, nm	0.3926(5)	0.3920 (−0.2%)	0.4096(3)	0.4110 (+0.3%)	0.4328(7)	0.4375 (+1.1%)
c, nm	0.801(5)	0.8154 (+1.8%)	0.8396(6)	0.8465 (+1.1%)	0.893(1)	0.8772 (−1.7%)
V, nm^3	0.1235	0.1253	0.1409	0.1430	0.1673	0.1679
Cm_z	0.27	0.2732	0.27	0.2734	0.271[a]	0.2769
Sl_z	0.63	0.6321	0.63	0.6322	0.633[a]	0.6297
Cm–M1, nm	0.2884	0.2877 (−0.2%)	0.3013	0.3037 (+0.8%)	0.3215[a]	0.3095 (−3.7%)
Cm–M1, nm	0.2889	0.2927 (+1.3%)	0.3015	0.3014 (0.0%)	0.3188[a]	0.3200 (+0.4%)
Cm–M2, nm	0.2921	0.2967 (+1.6%)	0.3050	0.3095 (+1.5%)	0.3240[a]	0.3269 (+0.9%)

The unit cell contains Cm on 2*c* (0, 1/2, Cm_z), M1 on 2*c* (0, 1/2, Sl_z), and M2 on 2*a* (0, 0, 0).

[a] Fractional coordinates were assumed by Damien et al. [34] to be the same as in $NdTe_2$.

[21]. The calculated value, 0.5875 nm, is 1.3% higher, exactly the same difference as in the CmS calculation. The calculated Cm–Se bond length is 0.2938 nm. CmSe is more clearly metallic than CmS based on the calculated density of electronic states.

Curium diselenide has the same tetragonal lattice as curium disulfide [33]. The calculated structure is compared to the experimental results in Table 8. The similarity between CmS_2 and $CmSe_2$ is clear from Table 8: the fractional coordinates of S and Se atoms in curium dichalcogenides are essentially identical, and the b/a ratios are the same within the 1% accuracy. $CmSe_2$ is more strongly metallic than other chalcogenides studied here.

3.4.3. Cm–Te compounds

Curium tellurides show all the same structural features as curium sulfides and selenides [34]. CmTe has a NaCl-type structure with $a = 0.6150(4)$ nm ($Fm\bar{3}m$, SG 225) [21,34]. Our calculation overestimates the cell parameter by 1.7%, $a = 0.6257$ nm, giving the Cm–Te bond length as 0.3128 nm. CmTe is metallic with roughly the same density of states at the Fermi level as CmSe.

The structure of $CmTe_2$ in the anti-Fe_2 As type tetragonal lattice is presented in Table 8 (P4/*nmm*, SG 129). This compound is also metallic, although with a lower density of electronic states at the Fermi level than CmTe. Magnetic moment is higher than in CmTe, probably due to a more localized character of charge density in $CmTe_2$. One expects a slightly more atomic-like charge density in $CmTe_2$ compared to CmTe since the bonds are noticeably longer in this compound.

The most tellurium rich curium telluride, $CmTe_3$, does not have known analogs in the family of curium chalcogenides. It crystallizes in the orthorhombic (pseudotetragonal) lattice (*Cmcm*, SG 63) [34]. The structure can be seen as composed of two ditelluride cells, shifted by $a/2$ and separated by an additional Te layer. Each curium atom is nine-fold coordinated with four bonds to Te1 (or Te3) atoms, and five bonds to Te2 atoms. A detailed comparison of the calculated and measured structures is given in Table 9.

Table 9
Theoretical and experimental structure of $CmTe_3$

	Experimental [34]	Theory
a, nm	0.434(2)	0.4315 (−0.6%)
b, nm	0.434(2)	0.4316 (−0.6%)
c, nm	2.57(1)	2.5434 (−1.0%)
V, nm^3	0.4841	0.4737
Cm_y	0.83[a]	0.8301
$Te1_y$	0.07[a]	0.0700
$Te2_y$	0.43[a]	0.4298
$Te3_y$	0.70[a]	0.7001
Cm–Te1×1, nm	0.3341	0.3308 (+0.8%)
Cm–Te1×4, nm	0.3164	0.3147 (0.0%)
Cm–Te2×2, nm	0.3364	0.3333 (+1.5%)
Cm–Te2×2, nm	0.3364	0.3333 (+1.5%)

The unit cell contains Cm on 4*c* (0, Cm_y, 1/4) and three Te atoms on 4*c* (0, Te_y, 1/4).

[a] Fractional coordinates were assumed to be the same as in $NdTe_3$ [34].

3.5. Curium pnictides

A number of curium pnictides CmX, where X = N, P, As, and Sb, have been synthesized [1,21]. More recently CmBi was produced [35], and furthermore its structure has been studied under applied pressure of up to 48 GPa [36].

All curium monopnictides crystallize in the NaCl structure. Theoretical and experimental lattice parameters are given in Table 10. The structures of these high-symmetry compounds are reproduced quite accurately in the calculations, with the deviations in lattice parameters not exceeding 0.5%.

Table 10
Theoretical and experimental lattice parameters of curium pnictides (nm)

	Experimental	Theory
CmN	0.5041(2) [37] 0.5027(1) [21]	0.5046
CmP	0.5725(5) [37] 0.5743(3) [21]	0.5771
CmAs	0.5901(6) [37] 0.5887(3) [21]	0.5906
CmSb	0.6248(5) [37] 0.6242(2) [21]	0.6251
CmBi	0.6333(1) [35] 0.6328(1) [36]	0.6328

All experimental data used ^{248}Cm, except for Ref. [37] where ^{244}Cm was used.

CmN, CmP, CmAs and CmSb have been shown experimentally to be ferromagnetic with the Curie temperatures of 109, 73, 88, and 162 K, respectively [1,38]. Magnetic moments for CmN and CmAs compounds were determined from these experiments as 7.02 and 6.58 μ_B/atom. Our calculations predict a ferromagnetic ground state for all of these compounds with effective magnetic moments of 7.24, 7.20, 6.80, 6.68, and 6.76 μ_B/atom when going from N to Bi. All these compounds are weakly metallic. The density of electronic states at the Fermi level increases monotonically with the ionic radius of a pnictogen, so that its value is twice higher in CmBi than in CmN.

3.5.1. CmBi phase diagram under pressure

The behavior of CmBi under pressure has been studied in detail [36]. A NaCl-type (B1-type, $Fm\bar{3}m$, SG 225) structure has been found to exhibit a first-order transition to a CsCl-type (B2-type, $Pm\bar{3}m$, SG 221) structure at 12 GPa, followed by a second-order transition to a tetragonal phase at 19 GPa. Theoretical analysis of the pressure dependence of the total energy gives the B1–B2 transition pressure as 14.2 GPa. This value is slightly higher than the experimental transition pressure, which is likely to be due to the neglect of thermal effects in the present calculations. The volume effect of the transition is twice smaller in the present calculations than was found experimentally, 8% instead of 16%. This difference, however, is within the uncertainty of the experimental data [36].

The accuracy of the calculation appears to be insufficient to make definite conclusions regarding the second observed transition, from the B2 phase to the LaSb-type tetragonal structure (P4/*mmm*, SG 123). However, a number of intriguing observations can be made. Let us summarize the experimental results regarding the B2 to tetragonal transition. This transition was found at 19 GPa on compression. The tetragonal phase remained stable on decompression and transformed directly to the B1 NaCl-type phase at 5 GPa. The reverse transition, tetragonal to B2, has never been observed [36].

Our results are based on the calculated pressure dependence of the enthalpies of the three phases of CmBi (Fig. 1). We found that the transition pressure from B2 to the tetragonal phase is only slightly above the pressure of the first transition, B1 to B2, and is about 15 GPa. This severely limits the region of stability of the B2 phase, from 14.2 to 15.3 GPa. This region can be seen as a small pocket where both curves on Fig. 1 have negative values. What is even more interesting is that the pressure dependence of the enthalpy difference between the B2 and the tetragonal phases is not monotonic. The tetragonal phase is more stable than the B2 phase from 0 to 8.8 GPa, and then again above 15.3 GPa. This observation would explain the large hysteresis effect observed experimentally, as well as the fact that on decompression tetragonal phase transforms directly to the B1 phase.

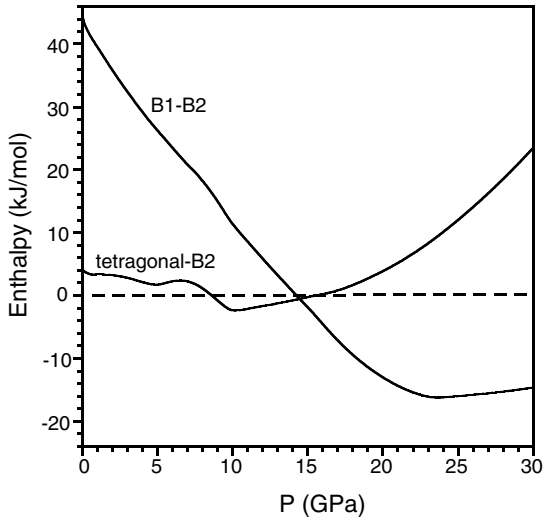

Fig. 1. Pressure dependence of the enthalpy differences between B1 and B2, and tetragonal and B2 structures of CmBi. Positive values correspond to the region of stability of the structure mentioned first, i.e., B1 phase is stable at low pressure, and tetragonal phase at high pressure.

We analyzed the high-pressure data for the B1, B2 and tetragonal polymorphs of CmBi using the third order Birch–Murnaghan equation of state. The values of the bulk modulus, B, and its pressure derivative, B', are given in Table 11. The good agreement with the experimental value for the bulk modulus of the B1 phase is typical for the DFT modeling of inorganic materials [7].

3.6. Curium oxides

Curium–oxygen phase diagram shows a rich variety of compounds, especially at elevated temperatures [1,39]. Cm_2O_3 alone exhibits five polymorphic forms, and there has been evidence for two additional intermediate phases between Cm_2O_3 and CmO_2, e.g. Cm_7O_{12} [39].

The simplest oxide structure is exhibited by CmO_2 that crystallizes in the fluorite lattice ($Fm\bar{3}m$, SG 225). Its lattice parameter at 15 K has been reported from neutron powder diffraction measurements as 0.5364(2) nm [40]. The calculated value is 2.8% higher at 0.5517 nm. Curium dioxide exhibits interesting magnetic properties. The effective magnetic moment of Cm^{4+} is zero, thus the tetravalent compounds of curium are expected to be paramagnetic. The experimental data, however, point to the magnetic moment from 2 to 4 μ_B/atom for Cm in CmO_2, the most accurate value being

Table 11
Equation of state parameters of CmBi compared with the experimental data [36]

	Experimental	Theory
B1 phase		
B, GPa	54(2)	49(1)
B'	7(1)	4.5(2)
B2 phase		
B, GPa	–	70(2)
B'	–	3.6(2)
Tetragonal phase		
B, GPa	–	58(4)
B'	–	4.1(3)

3.36 μ_B/atom [40]. The experimentally observed magnetic moment is often attributed to the presence of Cm^{III} and thus to the deviation from stoichiometry. Morss et al. [40] showed that this explanation is hardly satisfactory since diffraction and magnetization data would yield disparate stoichiometries. Our calculation gives α magnetic moment on Cm of 3.39 μ_B/atom thus suggesting that the itinerant magnetism picture based on delocalized electrons is more appropriate for this system than the description based purely on the crystal-field theory.

An example of the complex curium oxide structure that contains trivalent curium ions and is described very accurately at the DFT level of theory is Cm_2CuO_4. This material has an I4/*mmm* symmetry (SG 139) and has been extensively characterized using neutron diffraction, X-ray absorption and magnetic susceptibility measurements in the wide range of temperatures [41]. The structural parameters are presented in Table 12. The crystal structure is represented very accurately in the calculation, while the experimentally observed magnetic order is very different from the collinear ferromagnetic ground state of the present calculations. The true magnetic structure as determined using neutron diffraction has the spins in the *a*-*b* planes aligned parallel, while the spins in the adjacent planes are aligned antiparallel. This case together with various similar examples [10] shows that the details of the magnetic structure do not necessarily have a noticeable effect on the crystal structure.

The measured magnetic moment of Cm_2CuO_4 is 7.89 μ_B/atom, which is dominated by curium ions [41]. It is impossible to derive information about the Cu magnetic moment from experimental data, apart from the statement that it is expected to be small, of the order of 0.2–0.5 μ_B/atom. We obtained the moment of 6.84 μ_B/atom on Cm ions and 0.1 μ_B/atom on Cu ions, in qualitative agreement with the experimental observations. We find this compound to be essentially an insulator, with a narrow valence band (about 6 eV). The fine structure of the valence band is determined by two strong peaks, Cu 3*d* and Cm 5*f* that are found at 2.1 and 1.8 eV below the Fermi level. Analysis of the spatial distribution of the spin density confirms the result obtained using Mulliken analysis, namely that there is very little spin contribution from Cu atoms.

Table 12
Theoretical and experimental structure of Cm_2CuO_4

	Experimental, 35 K [41]	Theory
a, nm	0.39234(2)	0.3938 (+0.4%)
c, nm	1.20785(11)	1.2273 (+1.6%)
V, nm^3	0.1859	0.1903
Cm_z	0.3510	0.3508
Cm–O2×4, nm	0.23102	0.2336 (+1.1%)
Cm–O1×4, nm	0.26624	0.2691 (+1.1%)

The unit cell contains Cm on 4*e* (0, 0, Cm_z), O1 on 4*c* (0, 1/2, 0), O2 on 4*d* (0, 1/2, 1/4), and Cu on 2*a* (0, 0, 0).

3.7. Curium intermetallic compounds

This section reviews binary intermetallic compounds of curium that were synthesized in recent years. Apart from the fundamental interest in the properties of such materials, there is a certain amount of technological interest in Cm intermetallic compounds. For example, a ^{248}Cm–Pt alloy is used as core material for sealed neutron sources applied as a reference when certifying neutron sources and equipment for neutron measurement. Unsealed ^{244}Cm alpha-sources are produced for elemental analysis of space body rocks by means of alpha-particle back scattering and X-ray fluorescence. These sources are made of ^{244}Cm alloyed with platinum or silicon, iridium, rhodium, and nickel [42].

In most of the systems described below curium exhibits covalent or metallic bonding with a fairly high coordination number as opposed to mainly ionic compounds discussed so far.

3.7.1. Curium silicides

At least three stoichiometric curium silicides have been synthesized and their structures determined using X-ray diffraction: orthorhombic CmSi, hexagonal Cm_2Si_3, and tetragonal $CmSi_2$ [43,44]. In addition, a new tetragonal phase $CmSi_{1.88}$ has been reported [44]. Experimental techniques used by Radchenko et al. [44] involve high-temperature vapor deposition of Cm on Si, resulting in the mixture of curium silicides on the substrate. The earlier techniques resulted in the actual separation of different phases [43] and might be seen as more accurate. Both of these studies have used the ^{244}Cm isotope, and the authors reported intensive self-destruction in the lattice. The authors explicitly state that the accuracy of the data is low: in fact, positions of silicon atoms were simply assumed to be the same as in other silicides of *f*-elements. Theoretical reexamination of these structures is thus warranted. We have not examined hexagonal curium sesquisilicide, since its structure has been experimentally indexed as a defect AlB_2 structure. CASTEP can in principle handle disordered defects in the virtual crystal approximation [45], but the present study is restricted to the fully ordered compounds.

CmSi crystallizes in the orthorhombic space group P*bnm* (SG 62). We would like to point out that the P*nma* setting chosen by Weigel and Marquart [43] and used in the ICSD database is inconsistent with the quoted atomic coordinates and the values of the cell parameters. The structure as given by these authors contains unphysical Cm–Si distances of the order of 0.1 nm. A correct description of the structure based on a P*bnm*

setting is given in Table 13. We should note that the calculated lattice parameters deviate significantly from the ones reported experimentally. The discrepancy is certainly beyond the error limits of the computational technique, and out of line with the deviations we have obtained for other curium compounds. The only viable explanation is that there are further problems with the experimental data beyond the above mentioned wrong assignment of atomic coordinates in the P*nma* space group. For example, the bond lengths calculated for the experimentally reported structure (after correcting the orientation) are too long. One can discard the two longest Cm–Si distances in Table 13 as non-bonding interactions, which leaves an impossibly low coordination number of five for curium atoms. It is difficult to tell from our calculations whether CmSi can be indexed in a different space group, or whether the reported experimental data refer to a non-stoichiometric compound. Further theoretical and experimental work is required to solve the actual structure of curium monosilicide.

Tetragonal curium disilicide has been indexed in the space group $I4_1/amd$ (SG 141) [43]. The detailed structure is reported in Table 14. There is a noticeable discrepancy in the value of the *a* lattice parameter that deserves further analysis. The structure suggested for $CmSi_2$ experimentally contains curium atoms with very high silicon coordination. There are 12 relatively short Cm–Si bonds compared to the sevenfold coordination in CmSi, see Table 13. It is not unlikely that the actual compound, like many other curium compounds, has a high concentration of Si vacancies, which would effectively reduce the average coordination number of curium and also reduce the cell volume. The fully ordered stoichiometric disilicide would have the lattice constant closer to the one predicted by our calculations.

Curium disilicide is a good metal according to the present DFT analysis. This agrees well with the qualitative observation that $CmSi_2$ samples were bright silvery in appearance [43].

The conclusion based on the analysis of the Tables 13 and 14 is that the experimental data for curium silicides are unreliable, as was already stressed by Weigel and Marquart [43].

3.7.2. Curium–nickel compounds

Radchenko et al. reported the successful synthesis of various Cm–Ni compounds by high-temperature vapor deposition of Cm on Ni substrate [46]. This technique

Table 13
Theoretical and experimental structure of CmSi

	Experimental [43]	Experimental [44][a]	Theory
a, nm	0.595(9)	0.598(1)	0.5615 (−6.1%)
b, nm	0.828(12)	0.8283(5)	0.7746 (−6.5%)
c, nm	0.391(4)	0.3918(6)	0.3816 (−2.6%)
V, nm^3	0.1926	0.1941	0.1660
Cm_x	0.125	–	0.1254
Cm_y	0.180	–	0.1794
Si_x	0.611	–	0.6218
Si_y	0.028	–	0.0349
Cm–Si×2, nm	0.3044	–	0.2900 (−4.7%)
Cm–Si×2, nm	0.3111	–	0.2922 (−6.1%)
Cm–Si×1, nm	0.3155	–	0.3003 (−4.8%)
Cm–Si×1, nm	0.3205	–	0.3041 (−5.1%)
Cm–Si×1, nm	0.3309	–	0.3085 (−6.8%)

The unit cell contains Cm on 4*c* (Cm_x, Cm_y, 1/4) and Si on 4*c* (Si_x, Si_y, 1/4).
[a] Averaged between two reported sets of measurements.

Table 14
Theoretical and experimental structure of $CmSi_2$

	Experimental [43]	Experimental [44][a]	Theory
a, nm	0.396(1)	0.3972(5)	0.4125 (+3.9%)
b, nm	1.372(3)	1.364(8)	1.3640 (0.0%)
V, nm^3	0.2152	0.2152	0.2321
Si_z	0.417	–	0.4156
Cm–Si×4, m	0.3029	–	0.3059 (+1.0%)
Cm–Si×8, m	0.3025	–	0.3136 (+0.37%)

The unit cell contains Cm on 4*a* (0, 0, 0) and Si on 8*i* (0, 0, Si_z).
[a] Averaged between two reported sets of measurements.

produces a phase mixture that is difficult to analyze accurately. In addition, the use of ^{244}Cm isotope resulted in significant radiation damage.

The main phases identified in that experiment are hexagonal $Ni_{15}Cm_2$ or $Ni_{17}Cm_2$ ($Ni_{17}Th_2$-type) and hexagonal Ni_5Cm (Cu_5Ca-type). The structures of the first two of these compounds are too complex for a theoretical investigation, especially since there is no information about atomic coordinates. We studied the latter intermetallic compound, Ni_5Cm, in the P*6*/*mmm* space group (SG 191). The results summarized in Table 15 show the good agreement with the experimental data.

Radchenko et al. [46] found reflections from a primitive cubic phase which was tentatively identified as Ni_3Cm with the structure of the Cu_3Au type ($Pm\bar{3}m$, SG 221), $a = 0.4149(5)$ nm. We have obtained the lattice parameter of 0.3927 nm, which is 5.4% smaller. It has been seen throughout this paper that the DFT–GGA calculations usually overestimate interatomic distances and lattice parameters, a known feature of this approach [7]. We will return to the analysis of the strong underestimation of the lattice parameter of Ni_3Cm later, when discussing the results for the family of M_3Cm intermetallic compounds.

3.7.3. Curium–platinum compounds

Cm–Pt intermetallic compounds have been synthesized using various techniques [47–51]. Erdmann and Keller [47,50] obtained Pt_5Cm and described it as orthorhombic with the lattice of Pt_5Tb (or Pt_5Sm) type. Radchenko et al. [51] showed using regression analysis that indexing of the Pt_5Cm compound in a hexagonal system is preferred to the orthorhombic solution, and that the same applies to other Pt_5An actinide compounds (Pt_5Am, Pt_5Sm, etc.). These authors also noted rapid X-ray amorphization of all synthesized compounds of ^{244}Cm, the factor that made accurate structural determination very difficult.

Radchenko et al. reported the synthesis of hexagonal Pt_5Cm and gave its lattice parameters as $a = 0.5300(4)$ and $c = 0.4413(3)$ nm [47] or 0.5303(6) and 0.4418(4) nm [51]. A more recent study describes the products obtained by high-temperature vapor deposition of Cm on Pt substrate [49]. Pt_5Cm was indexed by Radchenko et al. [49] in the same Cu_5Ca-type hexagonal structure as Ni_5Cm (see above) with the same lattice parameters as reported earlier [48]. Our calculations show that the structures of hexagonal Pt_5Cm and Ni_5Cm are described theoretically with approximately the same accuracy (Table 15). The relative stability of the orthorhombic and hexagonal forms of Pt_5Cm is not addressed by the present study and deserves a separate investigation.

We find Ni_5Cm and Pt_5Cm to be good metals. Both *d*- and *f*-states contributions to electronic density of states have strong peaks in the valence band close to the Fermi level, E_F, resulting in high values of $N(E_F)$.

The high-temperature vapor deposition technique used by Radchenko et al. [49] allowed these authors to synthesize and characterize a few additional compounds such as Pt_2Cm and Pt_3Cm. Pt_2Cm has been indexed in the cubic Cu_2 Mg-type cell. The structure has the space group $Fd\bar{3}m$ (SG 227), with Pt atom on Wyckoff 16*c* position (1/8, 1/8, 1/8) and Cm atom on 8*b* position (1/2, 1/2, 1/2). The experimental lattice constant is 0.764(4) nm, and the calculated value is 0.7745 nm (+1.4%).

Pt_3Cm has a cubic Cu_3Au-type cell, space group $Pm\bar{3}m$ (SG 221), with Cm on 1*a* position (0, 0, 0) and Pt on 3*c* position (1/2, 1/2, 0). The calculated lattice constant is 0.4162 nm, which is 1.8% smaller than the experimental value of 0.424(7) nm [49]. The large experimental error reflects a number of factors: difficulty of indexing the structure from a small number of weak reflections, lattice damage due to the use of ^{244}Cm isotope, and most importantly the sample inhomogeneity which manifested itself as a strong dependence of the lattice parameter on the diffraction angle [49].

3.7.4. Curium–iridium and curium–rhodium compounds

Cm–Ir and Cm–Rh compounds are structurally very similar to the Cm–Pt ones. Cubic Ir_2Cm with the Cu_2Mg-type cell ($Fd\bar{3}m$, SG 227), has been found by Erdmann and Keller [50], $a = 0.7561$ nm, and by Radchenko et al., $a = 0.7571$ nm [49] and 0.75616(3) nm [52]. We obtained the value of 0.7599 nm that is only

Table 15
Theoretical and experimental structure of CmM_5, M = Ni or Pt

	$CmNi_5$		$CmPt_5$	
	Experimental [46][a]	Theory	Experimental [49]	Theory
a, nm	0.4869(2)	0.4968 (+2.0%)	0.53000(1)	0.5391 (+1.7%)
c, nm	0.402(1)	3.980 (−0.9%)	0.44133(2)	0.4441 (+0.6%)
V, nm^3	0.0825	0.0851	0.1074	0.1118
Cm–M1, nm	0.2811	0.2868 (+2.0%)	0.3060	0.3113 (+1.7%)
Cm–M2, nm	0.3157	0.3183 (+0.8%)	0.3448	0.3492 (+1.3%)

The unit cell contains Cm on 1*a* (0, 0, 0), M1 on 3*g* (1/2, 0, 1/2) and M2 on 2*c* (1/3, 2/3, 0).

[a] Averaged between two reported sets of measurements.

0.4% higher. A similar Rh_2Cm phase has been found with $a = 0.7502(8)$ [53] or 0.75187(5) nm [49]. The theoretical value is 0.7615 nm, or 1.3% higher.

Radchenko et al. [49] interpreted the reflexes of the Cu_3Au-type lattice in the Cm–Ir system as belonging to the Ir_3Cm phase, similar to the Pt_3Cm compound ($Pm\bar{3}m$, SG 221). Our calculated lattice parameter for this phase is 0.4061 nm, 2.7% lower than the experimental value of 0.4173(5) nm [49]. The similar phase, Rh_3Cm, in the Cm–Rh system was identified experimentally based on the set of weak reflections. The lattice parameter was reported as 0.418(1) [53] or 0.4161(1) nm [49] while our theoretical value is 2.9% lower at 0.4040 nm. An earlier result due to Erdmanm and Keller [50] gives $a = 0.4106$ nm in a slightly better agreement with our calculations.

The results for M_3Cm compounds with the reportedly Cu_3Au-type lattice merit a separate discussion. We have included Pd_3Cm in the comparison below (experimental values of the lattice parameter are $a = 0.4147(3)$ nm [50] and 0.4126(1) nm [54], calculated $a = 0.4082$ nm). The calculated lattice parameter of M_3Cm intermetallics where M = Ni, Pt, Ir, Rh, and Pd, is underestimated by the present calculations by 5.4%, 1.8%, 2.7%, 2.9%, and 1.6%, respectively. This systematic error cannot be due to the inherent features of the calculation (e.g., exchange-correlation functional, pseudopotentials, etc.) since we do not observe such clear and consistent trend for other compounds studied here. The systematic discrepancy of this magnitude might point to an underlying fundamental difficulty with the experimental assignment of Cu_3Au-type reflections to stoichiometric M_3Cm compounds, especially for M = Ni, Ir and Rh. The homogeneity range of these intermetallic compounds can be quite wide, up to 10% [55], which might account for some of the uncertainty of the experimental data. Another possible explanation of the large discrepancies could be that the lattice type for some of these fcc compounds is not actually Cu_3Au so that not all of the listed above M_3Cm compounds are isomorphic. Further experimental studies would be required to shed light on the actual structure of these compounds.

3.8. Reliability of the DFT results

It seems appropriate to return to the question of the accuracy of the calculations presented after surveying a wide variety of curium compounds. We have shown that the agreement between calculated and measured lattice parameters and interatomic distances is typically of the order of 1–2% which is consistent with the typically observed DFT accuracy [6,7]. This magnitude of an error is inherent to the approximations made in constructing exchange-correlation potentials within the DFT framework, which is further combined with errors introduced by the pseudopotential approximation. One should also keep in mind that DFT can potentially break down for systems with strongly localized highly correlated electrons. The results shown above confirm that 5*f* electrons of Cm are described satisfactorily within the DFT formalism.

Further sources of discrepancies between theory and experiment are numerous. On the theoretical side we could mention the limitations of the $T = 0$ K approach which completely neglects thermal effects (see discussion in Section 2). More importantly, the present results might be affected by the neglect of the spin–orbit interaction in the DFT Hamiltonian. The spin–orbit terms should have a stronger effect on the details of the electronic structure than on the crystal geometry, which was the main purpose of the present study. Incorrect ordering of magnetic moments is also a potential source of discrepancy. This is the most likely reason for the overestimation of the cell volume of antiferromagnetic hexagonal curium, which has been studied here with a ferromagnetic ordering. It is hoped that imminent methodological developments in this area will soon provide researchers with tools that describe accurately not only crystal structures but also magnetic ordering.

Experimental data, on the other hand, have to be treated cautiously in many cases. The main reasons for the errors and uncertainties in structure determination are related to deviations from stoichiometry. One has to take into account that such materials as intermetallic compounds of curium have sufficiently wide homogeneity ranges that might influence the measured lattice parameters.

4. Conclusions

We have presented a comprehensive density-functional study of curium and its compounds. Our calculations faithfully reproduce the structure and energetics of these crystals, thus providing reliable predictions for the structures that have not been solved experimentally (e.g., CmI_3 and CmF_3). On few occasions, as in the case of curium silicides and cubic M_3Cm intermetallic compounds, our results suggest the need for a reinterpretation of the available experimental data. The level of accuracy achieved here signifies the maturity of the theoretical methods and gives us confidence in the predictive power of modeling in solid state chemistry of actinides.

Actinide compounds are notoriously difficult to study experimentally, and thus ab initio modeling of their properties both at ambient conditions and under compression can be used to gain information about the structural features, defect properties, and phase diagrams of these materials. Specific examples of the additional insight into structure and properties of rare-earth compounds provided by the present study include the

first structure refinement of CmI_3 and CmF_3; a stability analysis of Cm hydrides that explains the difficulty of synthesizing CmH_3; an explanation of the observed features of the pressure-induced transformations in CmBi.

In the light of this study we expect that the pseudopotential DFT approach will increasingly complement the experimental techniques currently in use for the structural study of actinide-containing compounds.

Acknowledgement

We are grateful to Professor J.R. Peterson for his help in establishing the crystal structure of CmOCl and his encouragement in course of the present work.

References

[1] P.G. Eller, R.A. Penneman, in: J.J. Katz, G.T. Seaborg, L.R. Morss (Eds.), The Chemistry of the Actinide Elements, Chapman and Hall, NY, 1986, p. 962.
[2] D. Brown, Halides of the Lanthanides and Actinides, Wiley, London, 1968.
[3] M. Noé, J. Fuger, Inorg. Nucl. Chem. Lett. 7 (1971) 421.
[4] L.V. Sudakov, I.I. Kapshukov, A.Yu. Baranov, E.V. Shimbarev, N.V. Lyalyushkin, Radiokhimiya 4 (1977) 490.
[5] W. Kohn, Rev. Mod. Phys. 71 (1999) 1253.
[6] M.C. Payne, M.P. Teter, D.C. Allan, T.A. Arias, J.D. Joannopoulos, Rev. Mod. Phys. 64 (1992) 1045.
[7] V. Milman, B. Winkler, J.A. White, C.J. Pickard, M.C. Payne, E.V. Akhmatskaya, R.H. Nobes, Int. J. Quant. Chem. 77 (2000) 895.
[8] P. Söderlind, O. Eriksson, B. Johansson, J.M. Wills, Phys. Rev. B 50 (1994) 7291.
[9] P. Söderlind, R. Ahuja, O. Eriksson, B. Johansson, J.M. Wills, Phys. Rev. B 61 (2000) 8119.
[10] C.J. Pickard, B. Winkler, R.K. Chen, M.C. Payne, M.H. Lee, J.S. Lin, J.A. White, V. Milman, D. Vanderbilt, Phys. Rev. Lett. 85 (2000) 5122.
[11] D. Vanderbilt, Phys. Rev. B 41 (1990) 7892.
[12] J.P. Perdew, J.A. Chevary, S.H. Vosko, K.A. Jackson, M.R. Pederson, D.J. Singh, C. Fiolhais, Phys. Rev. B 46 (1992) 6671.
[13] J.A. White, D.M. Bird, Phys. Rev. B 50 (1994) 4954.
[14] J.P. Perdew, K. Burke, M. Ernzerhof, Phys. Rev. Lett. 77 (1996) 3865.
[15] P. Focher, G.L. Chiarotti, in: L. Reatto, F. Manghi (Eds.), Progress in Computational Physics of Matter, World Scientific, Singapore, 1995, p. 1.
[16] CASTEP User Guide, Accelrys Inc., San Diego, 2001.
[17] M.D. Segall, P.L.D. Lindan, M.J. Probert, C.J. Pickard, P.J. Hasnip, S.J. Clark, M.C. Payne, J. Phys.: Cond. Matter 14 (2002) 2717.
[18] R.J.M. Konings, J. Nucl. Mater. 298 (2001) 255.
[19] B. Kanellakopulos, J.P. Charvillat, F. Maino, W. Müller, in: W. Müller, R. Lindner (Eds.), Transplutonium Elements, North-Holland, Amsterdam, 1976, p. 181.
[20] P.G. Huray, S.E. Nave, J.R. Peterson, R.G. Haire, Physica 102B (1980) 217.
[21] D. Damien, R.G. Haire, J.R. Peterson, J. Less-Common Metals 68 (1979) 159;
J. Phys. Colloq. 40 (1979) C4.
[22] J.R. Peterson, J.H. Burns, J. Inorg. Nucl. Chem. 35 (1973) 1525.
[23] L.B. Asprey, T.K. Keenan, F.H. Kruse, Inorg. Chem. 4 (1965) 985.
[24] G.D. Del Cul, R.G. Haire, J.R. Peterson, J. Alloys Compd. 181 (1992) 63.
[25] B. Maximov, H. Schulz, Acta Crystallogr. B 41 (1985) 88.
[26] A. Zalkin, D.H. Thompson, Acta Crystallogr. B 41 (1985) 91.
[27] J.R. Peterson, J. Inorg. Nucl. Chem. 34 (1972) 1603.
[28] D.H. Templeton, C.H. Dawben, J. Amer. Chem. Soc. 75 (1953) 6069.
[29] S. Kern, J. Hayward, S. Roberts, J.W. Richardson Jr., F.J. Rotella, L. Soderholm, B. Cort, M. Tinkle, M. West, D. Hoisington, G.H. Lander, J. Chem. Phys. 101 (1994) 9333.
[30] B.M. Bansal, D. Damien, Inorg. Nucl. Chem. Lett. 6 (1970) 603.
[31] J.K. Gibson, R.G. Haire, J. Solid State Chem. 59 (1985) 317.
[32] J.K. Gibson, R.G. Haire, J. Phys. Chem. 94 (1990) 935.
[33] D. Damien, J.P. Charvillat, W. Müller, Inorg. Nucl. Chem. Lett. 11 (1975) 451.
[34] D. Damien, A. Wojakowski, W. Müller, Inorg. Nucl. Chem. Lett. 12 (1976) 441.
[35] J.K. Gibson, R.G. Haire, J. Less Common Metals 132 (1987) 149.
[36] M. Gensini, R.G. Haire, U. Benedict, F. Hulliger, Physica B 190 (1993) 75.
[37] J.P. Charvillat, U. Benedict, D. Damien, C.H. de Novion, A. Wojakowski, W. Müller, in: W. Müller, R. Lindner (Eds.), Transplutonium Elements, North-Holland, Amsterdam, 1976, p. 79.
[38] S.E. Nave, P.G. Huray, J.R. Peterson, D.A. Damien, R.G. Haire, Physica B 107 (1981) 253.
[39] R.P. Turcotte, T.D. Chikalla, L. Eyring, J. Inorg. Nucl. Chem. 35 (1973) 809.
[40] L.R. Morss, J.W. Richardson, C.W. Williams, G.H. Lander, A.C. Lawson, N.M. Edelstein, G.V. Shalimoff, J. Less Common Metals 156 (1989) 273.
[41] L. Soderholm, S. Skanthakumar, C.W. Williams, Phys. Rev. B 60 (1999) 4302.
[42] Radionuclide sources and preparations: Catalogue. SSC RIAR, Dimitrovgrad, 1996. Available from http://www.niiar.simbirsk.su/drsp/en/drsp.htm.
[43] F. Weigel, R. Marquart, J. Less Common Metals 90 (1983) 283.
[44] V.M. Radchenko, A.G. Seleznev, R.R. Droznik, M.A. Ryabinin, Radiochemistry 40 (1998) 4.
[45] B. Winkler, C.J. Pickard, V. Milman, Chem. Phys. Lett. 362 (2002) 266.
[46] V.M. Radchenko, A.G. Seleznev, M.A. Ryabinin, R.R. Droznik, V.Ya. Vasiliev, Radiokhimiya 37 (1995) 317.
[47] B. Erdmann, C. Keller, Inorg. Nucl. Chem. Lett. 7 (1971) 675.

[48] V.M. Radchenko, A.G. Seleznev, V.D. Shushakov, M.A. Ryabinin, L.S. Lebedeva, E.A. Karelin, V.Ya. Vasiliev, Radiokhimiya 27 (1985) 38.
[49] V.M. Radchenko, A.G. Seleznev, M.A. Ryabinin, R.R. Droznik, V.Ya. Vasiliev, Radiokhimiya 36 (1994) 299.
[50] B. Erdmann, C. Keller, J. Solid State Chem. 7 (1973) 40.
[51] V.M. Radchenko, V.D. Shushakov, M.A. Ryabinin, A.G. Seleznev, T.V. Shushakova, V.Ya. Vasiliev, Radiokhimiya 25 (1983) 649;
V.M. Radchenko, V.D. Shushakov, A.G. Seleznev, M.A. Ryabinin, L.S. Lebedeva, V.Ya. Vasiliev, V.M. Nikolayev, J. Less Common Metals 157 (1990) 147.
[52] V.M. Radchenko, A.G. Seleznev, M.A. Ryabinin, R.R. Droznik, E.N. Shiryaev, V.D. Shushakov, V.Ya. Vasiliev, Radiokhimiya 34 (1992) 1.
[53] V.M. Radchenko, A.G. Seleznev, M.A. Ryabinin, R.R. Droznik, V.D. Shushakov, V.Ya. Vasiliev, Radiokhimiya 35 (1993) 25.
[54] V.M. Radchenko, M.A. Ryabinin, N.Yu. Nesgovorov, E.V. Shimbarev, L.V. Sudakov, I.I. Kapshukov, V.Ya. Vasiliev, Radiokhimiya 24 (1982) 92.
[55] V.M. Radchenko, A.G. Seleznev, L.S. Lebedeva, R.R. Droznik, M.A. Ryabinin, V.D. Shushakov, Radiokhimiya 31 (1989) 1.